3D FE Discontinuous Sheet for Microwave Heating

R.A. Ehlers and A.C. Metaxas

***Abstract*— The article presents a method for modelling the EM properties of thin metallic films typical of electromagnetically active food packages within multimode microwave applicators. A discontinuous sheet with 6 degrees of freedom (DOF) is incorporated within a time or frequency domain edge FE formulation by splitting the tetrahedral-element discretized domain on the thin film surface and adding new DOF. Superior accuracy is observed when comparing with existing surface sheet conditions. Thermal image validation is provided for multimode applications.**

***Index Terms*— Thin conducting film, metallic sheet, finite edge element, microwave package.**

I. Introduction

THE use of the approximate boundary conditions such as the Standard Impedance Boundary Condition (SIBC) proposed by Leontovich [1] have seen extensive use in electromagnetic (EM) applications for many years. Although these conditions are satisfactory for representing highly reflective surfaces, they fail as the surface becomes more transmittive. The resistive sheet [2] and the so-called modified resistive sheet [3], are however able to account for the transmitted field component, although with a loss in accuracy as shown later. Improved accuracy is brought about by making use of a dual surface method which has been seen for the finite difference time domain (FDTD) [4] as well as for a 2D finite element (FE) application [5]. However, no application of a dual surface method for modelling thin films using the FE method has been seen in 3D. The focus of this paper is hence to introduce such a method and present results of its application within a microwave heating context [6].

II. Thin film boundary conditions

The impedance as used in a modification of the SIBC extended to incorporate the film thickness, τ, is given as [7]

$$Z_{in} = Z_f \frac{Z_0 + Z_f \tanh(\gamma_1 \tau)}{Z_f + Z_0 \tanh(\gamma_1 \tau)} \quad (\Omega) \tag{1}$$

where the film impedance, Z_f, for a conductivity, σ_f, is defined as

$$Z_f = (1+\jmath)\sqrt{\frac{\omega\mu}{2\sigma_f}} \quad (\Omega) \tag{2}$$

The complex propagation constant for a non-magnetic metal is expanded, with f being the frequency, as

$$\gamma_1 = (1+\jmath)\sqrt{\pi\mu_0 f \sigma_f} \quad (\mathrm{m}^{-1}) \tag{3}$$

With reference to figure 1, alternative thin film boundary conditions are described. The resistive sheet condition, which assumes continuity in the tangential electric field, $E_{t1} = E_{t2}$, is

$$\mathbf{n}\times\mathbf{n}\times\mathbf{E} = -Z_{res}[\mathbf{n}\times\mathbf{H}]^+_- \tag{4}$$

where Z_{res} is the sheet impedance given by

$$Z_{res} = \frac{-\jmath}{\omega\epsilon_0\tau(\epsilon_r - 1)} \quad (\Omega) \tag{5}$$

and the permittivity is expanded as $\epsilon_r = \epsilon^{'} - \jmath\epsilon^{''}$ in which $\epsilon^{''}$ is understood to represent all possible material losses. In the modified resistive sheet, the discontinuity in the electric field is accounted for, that is $E_{t1} \neq E_{t2}$

$$\mathbf{E_{t2}} = \alpha\mathbf{E_{t1}} \tag{6}$$

where

$$\alpha = \cos(\gamma_2\tau) + \frac{1}{Z_0}\left(\frac{\jmath\omega\mu}{\gamma_2}\right)\sin(\gamma_2\tau) \tag{7}$$

and $\gamma_2 = \omega\sqrt{\mu\epsilon_0\epsilon_r}$.

Unlike any of the methods already described where the same surface (Γ_{res} or Γ_{modres}) represents components of incident and transmitted fields, the discontinuous sheet introduces additional degrees of freedom by way of a dual surface (Γ_1 and

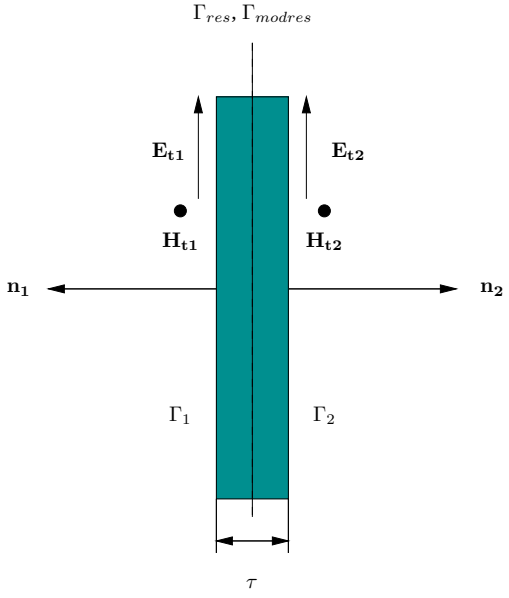

Fig. 1. Tangential field components either side of a thin film surface, as used in the resistive, modified resistive and discontinuous sheets.

The authors are with the Electricity Utilisation Group, Engineering Department, University of Cambridge, Cambridge, CB2 1PZ, UK (rae@cantab.net, acm@metaxas-associates.com)

Γ_2) representation of the thin film surface where the following transmission line equalities hold

$$\begin{bmatrix} \mathbf{E_{t1}} \\ \mathbf{E_{t2}} \end{bmatrix} = \begin{bmatrix} Z_{11} & -Z_{12} \\ Z_{12} & -Z_{11} \end{bmatrix} \begin{bmatrix} \mathbf{n_1} \times \mathbf{H_{t1}} \\ \mathbf{n_2} \times \mathbf{H_{t2}} \end{bmatrix} \tag{8}$$

The impedances Z_{11} and Z_{12} are given as [4]

$$Z_{11} = \frac{-\jmath\omega\mu}{\gamma_2 \tan(\gamma_2\tau)} \quad \text{and} \quad Z_{12} = \frac{-\jmath\omega\mu}{\gamma_2 \sin(\gamma_2\tau)} \tag{9}$$

The numerical implementation of the discontinuous sheet is discussed next for both the frequency and time domains where all mediums are considered to be homogeneous. The implementation requires that the mesh representing the computation domain is split on the relevant thin film structure(s) such that the film surface can be duplicated, creating additional degrees of freedom. Two surface integral terms are required within the numerical formulation, each of which is responsible for modelling the tangential field components on one of the two surfaces resulting from the split mesh. To link the mesh again, a thin film element of the discontinuous sheet is thus required to have six degrees of freedom - three for each surface integral term.

III. Frequency domain formulation

Equation 8 can be rewritten in terms of the magnetic field components as

$$\begin{bmatrix} \mathbf{n_1} \times \mathbf{H_1} \\ \mathbf{n_2} \times \mathbf{H_2} \end{bmatrix} = \begin{bmatrix} \frac{Z_{11}}{Z_{11}^2 - Z_{12}^2} & \frac{-Z_{12}}{Z_{11}^2 - Z_{12}^2} \\ \frac{-Z_{12}}{Z_{11}^2 - Z_{12}^2} & \frac{Z_{11}}{Z_{11}^2 - Z_{12}^2} \end{bmatrix} \begin{bmatrix} \mathbf{E_{t1}} \\ \mathbf{E_{t2}} \end{bmatrix} \tag{10}$$

Manipulating Maxwell's equation, the Helmholtz equation is derived which is then modified to include two surface integrals as follows

$$\frac{1}{\mu}\int_\Omega (\nabla \times \psi)\cdot(\nabla \times \mathbf{E})d\Omega - \omega^2\epsilon_0\epsilon_r \int_\Omega \psi \cdot \mathbf{E} d\Omega =$$

$$-\jmath\omega \int_\Omega \psi \cdot \mathbf{J_s} + \jmath\omega \int_{\Gamma 1} \psi \cdot (\mathbf{n_1} \times \mathbf{H_{t1}}) d\Gamma 1$$

$$+\jmath\omega \int_{\Gamma 2} \psi \cdot (\mathbf{n_2} \times \mathbf{H_{t2}}) d\Gamma 2 \tag{11}$$

where $\mathbf{J_s}$ represents the microwave cavity source excitation. Substituting equation 10 into equation 11 and making use of edge elements, the frequency domain edge element discretised formulation including the discontinuous sheet is

$$[\mathbf{S}]\mathbf{e} - \gamma_0^2[\mathbf{T}]\mathbf{e} - [\mathbf{D_{dis}}]\mathbf{e} = \mathbf{b} \tag{12}$$

where the stiffness and mass matrices are represented by $[\mathbf{S}]$ and $[\mathbf{T}]$ respectively, $\mathbf{e}$ is the vector of unknown edge values and $\mathbf{b}$ denotes the source vector. The matrix, $\mathbf{D_{dis}}$, represents the surface integrals of equation 11 and is expanded, together with the electric field as

$$[\mathbf{D_{dis}}]\mathbf{e} = [\mathbf{D_1}]\mathbf{e_{1-3}} - [\mathbf{D_2}]\mathbf{e_{4-6}}$$

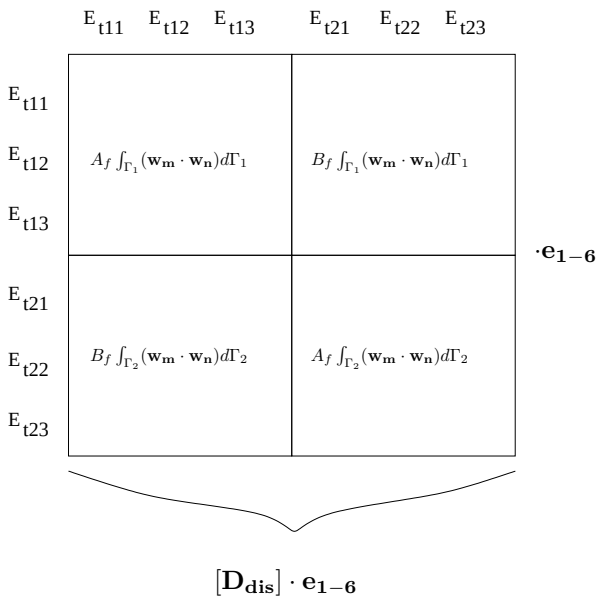

Fig. 2. Thin fi lm element matrix used for the frequency domain discontinuous sheet.

$$-[\mathbf{D_3}]\mathbf{e_{1-3}} + [\mathbf{D_4}]\mathbf{e_{4-6}} \tag{13}$$

The matrix and vector entries corresponding to an individual element are

$$[\mathbf{D_1}]^e_{m,n}\, {e_m}^e = \frac{\jmath\omega Z_{11}}{Z_{11}^2 - Z_{12}^2}\int_{\Gamma 1}(\mathbf{w_{1-3}}\cdot\mathbf{w_{1-3}})\mathbf{e_{1-3}}d\Gamma 1 \tag{14}$$

$$[\mathbf{D_2}]^e_{m,n}\, {e_m}^e = -\frac{\jmath\omega Z_{12}}{Z_{11}^2 - Z_{12}^2}\int_{\Gamma 1}(\mathbf{w_{1-3}}\cdot\mathbf{w_{4-6}})\mathbf{e_{4-6}}d\Gamma 1 \tag{15}$$

$$[\mathbf{D_3}]^e_{m,n}\, {e_m}^e = -\frac{\jmath\omega Z_{12}}{Z_{11}^2 - Z_{12}^2}\int_{\Gamma 2}(\mathbf{w_{4-6}}\cdot\mathbf{w_{1-3}})\mathbf{e_{1-3}}d\Gamma 2 \tag{16}$$

$$[\mathbf{D_4}]^e_{m,n}\, {e_m}^e = \frac{\jmath\omega Z_{11}}{Z_{11}^2 - Z_{12}^2}\int_{\Gamma 2}(\mathbf{w_{4-6}}\cdot\mathbf{w_{4-6}})\mathbf{e_{4-6}}d\Gamma 2 \tag{17}$$

where $\mathbf{e_{1-3}}$ and $\mathbf{e_{4-6}}$ are vector entries of the electric field circulation on each of the two triangular surfaces of the thin film element. The corresponding basis functions are given by $\mathbf{w_{1-3}}$ and $\mathbf{w_{4-6}}$ respectively.

The thin film element consists of a single matrix comprised of contributions from each of the four matrices and corresponding vector entries, from equation 13, with a total of six degrees of freedom as shown in figure 2. The coefficients in figure 2 are given as

$$A_f = \frac{\jmath\omega Z_{11}}{Z_{11}^2 - Z_{12}^2} \quad \text{and} \quad B_f = -\frac{\jmath\omega Z_{12}}{Z_{11}^2 - Z_{12}^2} \tag{18}$$

In figures 2, 3 and 4, $\mathbf{w_m}$ and $\mathbf{w_n}$ correspond to the basis functions of edges m and n respectively. Furthermore, the tangential electric field indices on the two surfaces of the thin film element are given by $E_{t1(1-3)}$ and $E_{t2(1-3)}$.

IV. Time domain formulation

The wave equation, which is derived from Maxwell's equations in the time domain, is supplemented with two surface integral terms, Γ_1 and Γ_2, that are required for the discontinuous sheet. The use of a first order absorbing boundary condition (ABC) is adopted in the time domain in order to represent an iso-circulator that protects the magnetron source from cavity reflections. The ABC is evaluated by adding an additional surface integral term, Γ_{ABC}, to the wave equation [11]

$$\frac{1}{\mu}\int_{\Omega}(\nabla\times\psi)\cdot(\nabla\times\mathbf{E})d\Omega+\sigma\int_{\Omega}\psi\cdot\frac{\partial\mathbf{E}}{\partial t}d\Omega$$

$$+\epsilon_0\epsilon^{'}\int_{\Omega}\psi\cdot\frac{\partial^2\mathbf{E}}{\partial t^2}d\Omega-\int_{\Gamma 1}\psi\cdot(\mathbf{n_1}\times\jmath\omega\mathbf{H_{t1}})d\Gamma_1$$

$$-\int_{\Gamma 2}\psi\cdot(\mathbf{n_2}\times\jmath\omega\mathbf{H_{t2}})d\Gamma_2=-\int_{\Omega}\psi\cdot\frac{\partial\mathbf{J_s}}{\partial t}d\Omega$$

$$+\int_{\Gamma_{ABC}}\psi\cdot(\mathbf{n}\times\frac{\partial\mathbf{H}}{\partial t})d\Gamma_{ABC} \tag{19}$$

where σ is understood to describe both the conductive and dipolar loss mechanisms within the dielectric material. Substituting for the electric field from the discontinuous sheet condition in equation 10, the surface integrals, Γ_1 and Γ_2 shown in the above equation, are rewritten as

$$-\int_{\Gamma_1}\psi\cdot A_f\mathbf{E_{t1}}d\Gamma_1-\int_{\Gamma_1}\psi\cdot B_f\mathbf{E_{t2}}d\Gamma_1$$

$$-\int_{\Gamma_2}\psi\cdot B_f\mathbf{E_{t1}}d\Gamma_2-\int_{\Gamma_2}\psi\cdot A_f\mathbf{E_{t2}}d\Gamma_2 \tag{20}$$

where A_f and B_f are the complex coefficients given by equation 18 which can be separated into real (A_r and B_r) and imaginary (A_i and B_i) components

$$-\int_{\Gamma_1}\psi\cdot\jmath\omega(A_r+\jmath\omega\frac{A_i}{\omega})\mathbf{E_{t1}}d\Gamma_1$$

$$+\int_{\Gamma_1}\psi\cdot\jmath\omega(B_r+\jmath\omega\frac{B_i}{\omega})\mathbf{E_{t2}}d\Gamma_1$$

$$+\int_{\Gamma_2}\psi\cdot\jmath\omega(B_r+\jmath\omega\frac{B_i}{\omega})\mathbf{E_{t1}}d\Gamma_2$$

$$-\int_{\Gamma_2}\psi\cdot\jmath\omega(A_r+\jmath\omega\frac{A_i}{\omega})\mathbf{E_{t2}}d\Gamma_2 \tag{21}$$

Since the cavity excitation and operation is at a single frequency, the coefficients A_r, B_r, A_i and B_i are constants. Transforming to the time domain yields

$$-A_r\int_{\Gamma_1}\psi\cdot\frac{\partial\mathbf{E_{t1}}}{\partial t}d\Gamma_1+B_r\int_{\Gamma_1}\psi\cdot\frac{\partial\mathbf{E_{t2}}}{\partial t}d\Gamma_1$$

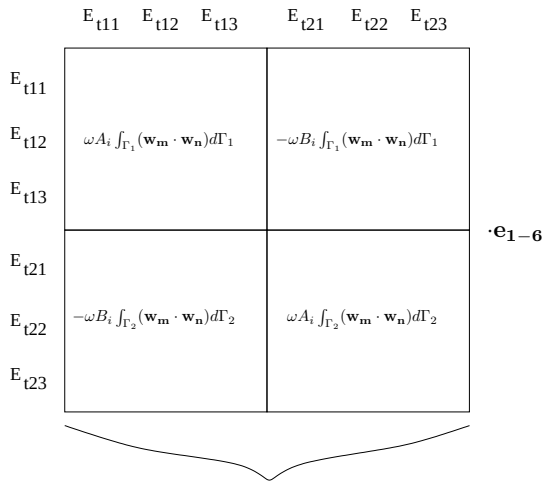

Fig. 3. Thin film elemental matrix with no field temporal derivative term used for the time domain discontinuous sheet.

$$+A_i\int_{\Gamma_1}\psi\cdot\omega\mathbf{E_{t1}}d\Gamma_1-B_i\int_{\Gamma_1}\psi\cdot\omega\mathbf{E_{t2}}d\Gamma_1$$

$$+B_r\int_{\Gamma_2}\psi\cdot\frac{\partial\mathbf{E_{t1}}}{\partial t}d\Gamma_2-A_r\int_{\Gamma_2}\psi\cdot\frac{\partial\mathbf{E_{t2}}}{\partial t}d\Gamma_2$$

$$-B_i\int_{\Gamma_2}\psi\cdot\omega\mathbf{E_{t1}}d\Gamma_2+A_i\int_{\Gamma_2}\psi\cdot\omega\mathbf{E_{t2}}d\Gamma_2 \tag{22}$$

where the constant ω represents the fixed operating frequency. Discretising using edge elements, the time domain matrix representation including the discontinuous sheet is

$$[\mathbf{S}]\mathbf{e}+[\mathbf{T}_\sigma]\frac{\partial\mathbf{e}}{\partial t}+[\mathbf{T}_\epsilon]\frac{\partial^2\mathbf{e}}{\partial t^2}$$

$$+[\mathbf{C_{ABC}}]\frac{\partial\mathbf{e}}{\partial t}+[\mathbf{C_{dis1}}]\mathbf{e}+[\mathbf{C_{dis2}}]\frac{\partial\mathbf{e}}{\partial t}\quad=\quad\mathbf{b} \tag{23}$$

where $[\mathbf{S}]$ is the stiffness matrix, $[\mathbf{T}_\sigma]$ together with $[\mathbf{T}_\epsilon]$ represent the mass matrices and $[\mathbf{C_{ABC}}]$ denotes the contribution of the absorbing boundary. The thin film matrices, $[\mathbf{C_{dis1}}]$ and $[\mathbf{C_{dis2}}]$, are assembled using equation 22 and shown together with their corresponding electric field edge value terms in figures 3 and 4, respectively [9]. The elemental matrices have six degrees of freedom, three for each surface, assuming a tetrahedral mesh is used. For each thin film element, two elemental matrices are added to the global matrix. Using the Newmark time stepping method [10], the film element entries, $[\mathbf{C_{dis1}}]$ and $[\mathbf{C_{dis2}}]$, for the field at the current time step, denoted by subscript *n+1*, and its relation to the previous two time steps, denoted by subscripts *n* and *n-1*, are added to the existing scheme as

$$[[\mathbf{T}_\epsilon]+\gamma_t\Delta t([\mathbf{T}_\sigma]+[\mathbf{C_{dis2}}])+\beta_t\Delta t^2([\mathbf{S}]$$

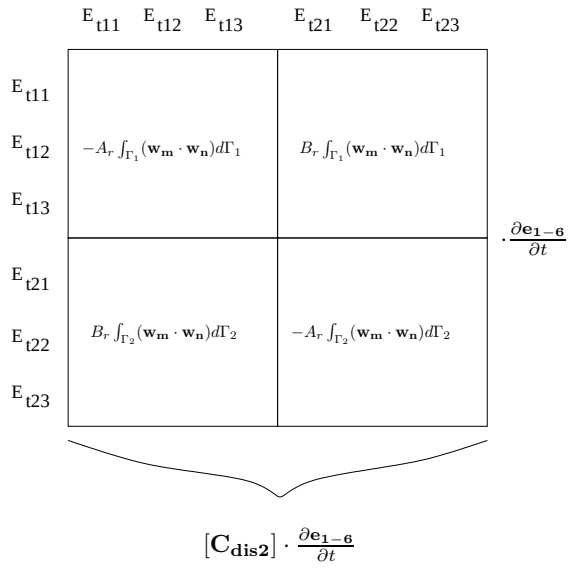

Fig. 4. Thin film elemental matrix with field first temporal derivative term used for the time domain discontinuous sheet.

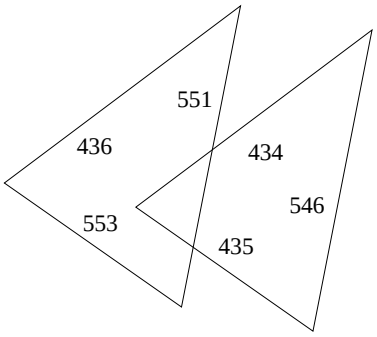

Fig. 5. Pure discontinuous sheet element. The numbers beside each edge are random and represent typical global matrix edge index entries.

$$+[\mathbf{C_{dis1}}])]\mathbf{e_{n+1}} = [2[\mathbf{T}_\epsilon] - (1-2\gamma_t)\Delta t([\mathbf{T}_\sigma] + [\mathbf{C_{dis2}}])$$

$$-(0.5+\gamma_t-2\beta_t)\Delta t^2([\mathbf{S}]+[\mathbf{C_{dis1}}])]\mathbf{e_n} + [-[\mathbf{T}_\epsilon]$$

$$-(\gamma_t-1)\Delta t([\mathbf{T}_\sigma]+[\mathbf{C_{dis2}}]) - (0.5+\gamma_t+\beta_t)\Delta t^2([\mathbf{S}]$$

$$+[\mathbf{C_{dis1}}])]\mathbf{e_{n-1}} + \Delta t^2[\beta_t \mathbf{b_{n+1}}$$

$$+(0.5+\gamma_t-2\beta_t)\mathbf{b_n} + (0.5-\gamma_t+\beta_t)\mathbf{b_{n-1}}] \qquad (24)$$

where the Newmark parameters $\beta_t = 0.25$ and $\gamma_t = 0.5$ are chosen to provide unconditional stability [8]. The use of equation 22 relies on the fact that a single operating frequency is used in the oven. The justification for the time domain implementation of the discontinuous sheet is due to the fact that the time domain is able to deal faster and more efficiently with the ill-conditioned matrices arising from multimode applicator heating problems than the frequency domain [8].

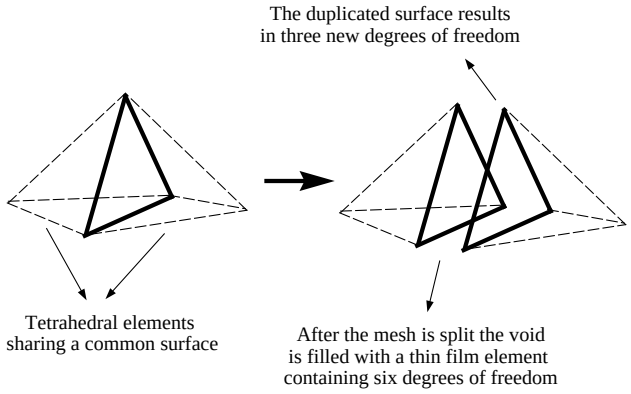

Fig. 6. Splitting of a tetrahedral mesh to include a thin film element.

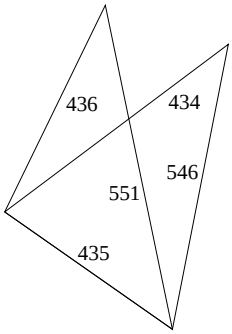

Fig. 7. Hybrid discontinuous-resistive sheet element. The numbers beside each edge are random and represent typical global matrix edge index entries.

V. Implementation

Figure 5 depicts the global numbering of a split surface as is required for a discontinuous sheet implementation. The process of splitting a mesh on a surface that belongs to two tetrahedral elements in order to include a thin film element is depicted in figure 6. The impedance weighting, denoted by the variables A and B, of the thin film element used to fill the void is shown in figure 8 together with the six degrees of freedom, e1-e6, that correspond to the edges of both surfaces in figure 5. These variables A and B were defined in figure 2 for the frequency domain and figures 3 and 4 for the time domain where A denotes the top left and bottom right matrix entries and B denotes the top right and bottom left entries. The global matrix contributions of these impedance coefficients are shown for the respective degrees of freedom in figure 10. Such an implementation for a thin film element constitutes a pure discontinuous application.

Where the geometry adopting the thin film surface is coupled to the surrounding mesh structure, a common degree of freedom is required as shown in figure 7. The latter describes the use of a hybrid discontinuous-resistive sheet, where the impedance weighting of the common edge, R, corresponds to that of a resistive sheet. A typical thin film element impedance matrix for such a hybrid sheet is shown in figure 9 where the global matrix contributions are shown in figure 11.

	1	2	3	4	5	6	
1	A	A	A	-B	-B	-B	e1
2	A	A	A	-B	-B	-B	e2
3	A	A	A	-B	-B	-B	e3
4	-B	-B	-B	A	A	A	e4
5	-B	-B	-B	A	A	A	e5
6	-B	-B	-B	A	A	A	e6

Fig. 8. Pure discontinuous sheet element impedance matrix showing link between the edge components. The numbers 1 to 6 denote the matrix row and column indices.

	1	2	3	4	5	6	
1	R/2	$\frac{A-B}{2}$	$\frac{A-B}{2}$	R/2	$\frac{A-B}{2}$	$\frac{A-B}{2}$	e1
2	$\frac{A-B}{2}$	A	A	$\frac{A-B}{2}$	-B	-B	e2
3	$\frac{A-B}{2}$	A	A	$\frac{A-B}{2}$	-B	-B	e3
4	R/2	$\frac{A-B}{2}$	$\frac{A-B}{2}$	R/2	$\frac{A-B}{2}$	$\frac{A-B}{2}$	e4
5	$\frac{A-B}{2}$	-B	-B	$\frac{A-B}{2}$	A	A	e5
6	$\frac{A-B}{2}$	-B	-B	$\frac{A-B}{2}$	A	A	e6

Fig. 9. Hybrid discontinuous-resistive fi lm element impedance matrix used on the fi lm boundary. The numbers 1 to 6 denote the matrix row and column indices.

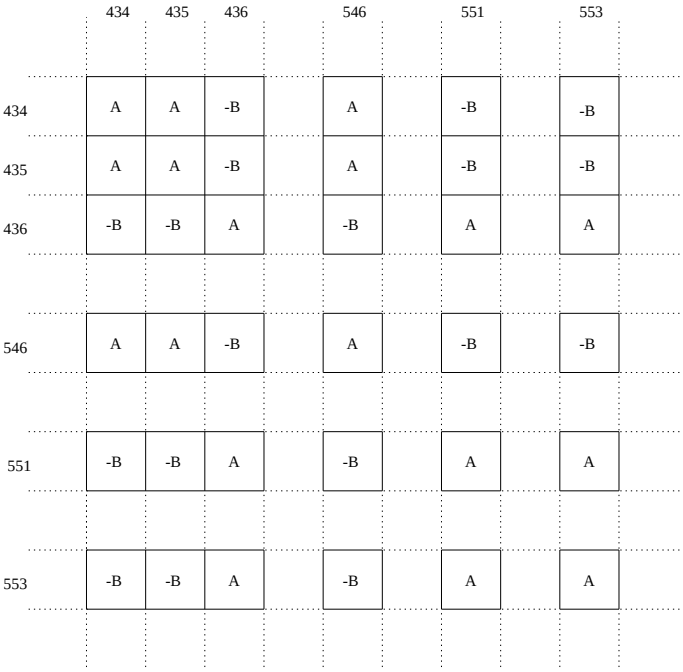

Fig. 10. Typical global matrix entries for a fi lm element confi guration shown in fi gure 5.

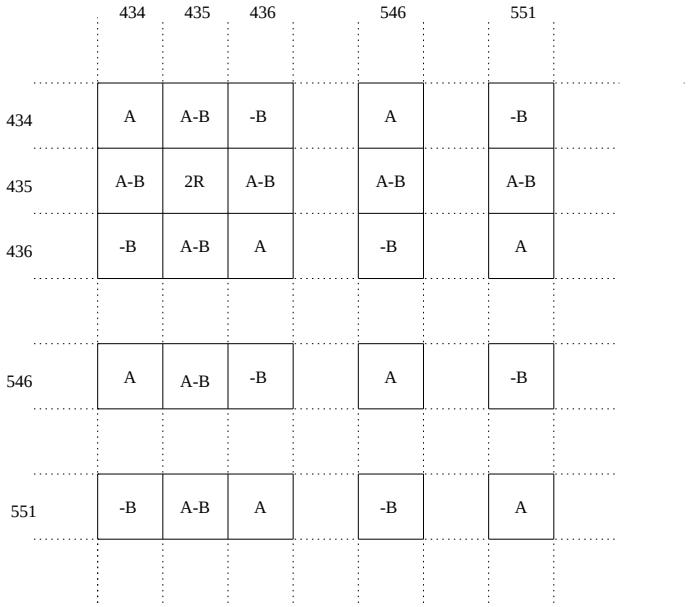

Fig. 11. Typical global matrix entries for a fi lm boundary element confi guration shown in fi gure 7.

VI. Results

A. Analytical - forward travelling waveguide

Validation is obtained using analytical expressions within a forward travelling WG9A waveguide (x=8.6 cm $\times$ y=4.3 cm $\times$ z=40 cm) operating at 2450 MHz [12]. A thin film is placed midway (z=20 cm) between the source (z=0 cm) and a reflectionless termination to the waveguide (z=40 cm). The reflection coefficient is compared with each of the four boundary methods discussed in section II using a range of film thicknesses constituting reflective and transparent thin film properties. These are shown for a film of conductivity 1.326e5 S/m in figure 12. The superior performance of the discontinuous sheet is evident which is shown with reflected, absorbed and transmitted power coefficients in figure 13.

B. Thermal imaging - multimode resonant applicator

With the lack of available analytical expressions to accurately represent a multimode heating system, a thermal imaging technique is used for validation. An image of the radiated thermal energy from the surface of an experimentally heated load is used as a qualitative representation of the dissipated power within the load. This can be compared with load surface power density obtained from the numerical result for the electric field distribution. All numerical simulations are carried out on a Pentium II, 450 MHz processor. Three active package configurations, using aluminium foil (3.77e7 S/m) of thickness 6.4 μm, are considered in a multimode cavity, where the setup for the first configuration is shown in figure 14. Other film thicknesses and conductivities may also be used depending on the application for which the thin film is required. The thin film substrate provides structural support but it is not modelled as it is assumed to be microwave transparent. The active pack, as seen from figure 15, provides shielding on the package side walls

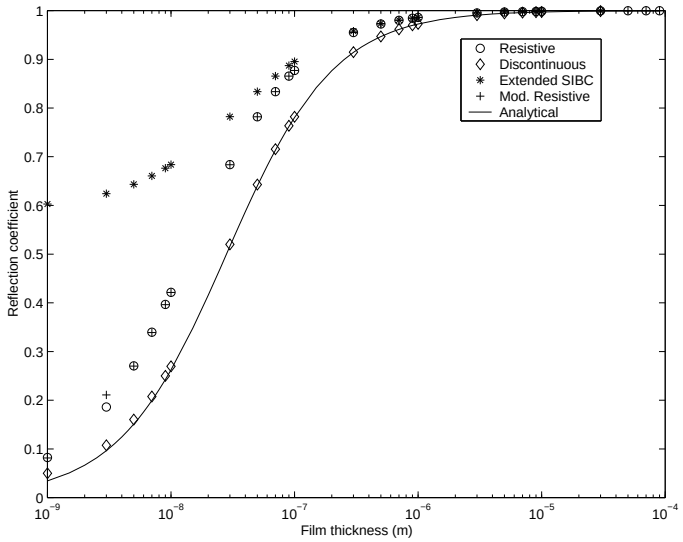

Fig. 12. Comparison of the extended SIBC, resistive sheet, modified resistive sheet and discontinuous sheet with the analytical equivalent.

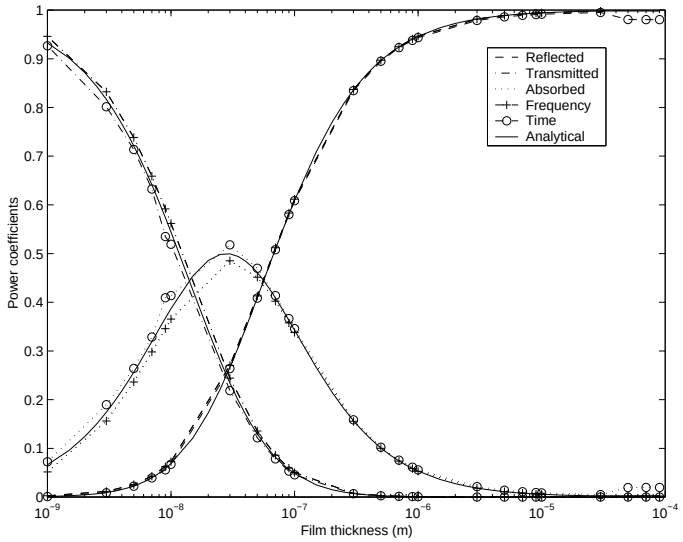

Fig. 13. Power coefficients of the discontinuous sheet as a function of thin film thickness.

and an antenna pattern arrangement at the base that is open-circuited for safety precautions when the package is unloaded. When loaded with a food product such as mashed potato ($55 - j26.5$), these structures are linked together using the ionic properties of the load. The resulting pattern at the base of the package is shown for the numerical power density and experimental thermal image in figure 16. The numerical result, which consisted of 684955 DOF, was obtained after 32 hours and 30 minutes using a convergence criterion of 4% change between successive cycles in the time domain.

The second configuration is aimed at studying the shielding performance of the package in figure 17, where half of the base is shielded for protecting microwave sensitive loads whilst loads requiring more exposure to microwave energy are placed in the unshielded zone of the package. The corresponding nu-

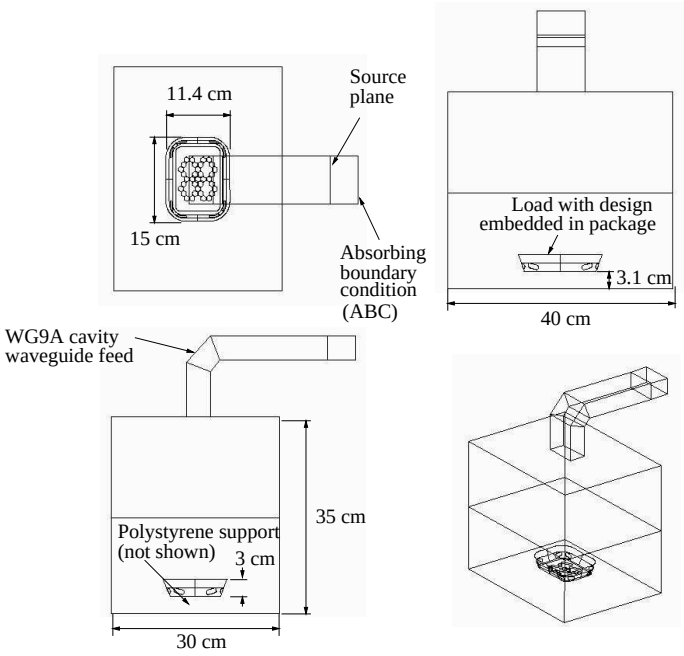

Fig. 14. Multimode oven setup used for experimental and numerical analysis.

Fig. 15. Food package design with open-circuited antenna base pattern.

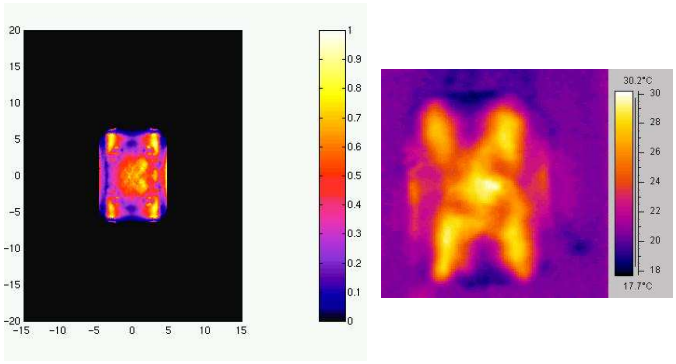

(a) Numerical (b) Thermal image

Fig. 16. Food surface plot at the base of the aluminium film package shown in figure 15.

Fig. 17. Food package design with shielding in base pattern.

merical and experimental results are shown, using a 4% convergence criterion, in figure 18, where the package was loaded with a new preparation of mashed potato (57 - j28). The simulation time was 30 hours and 32 minutes whilst the total number of DOF was 686882. The effects of thermal diffusion can be observed from the thermal image (figure 18(b)).

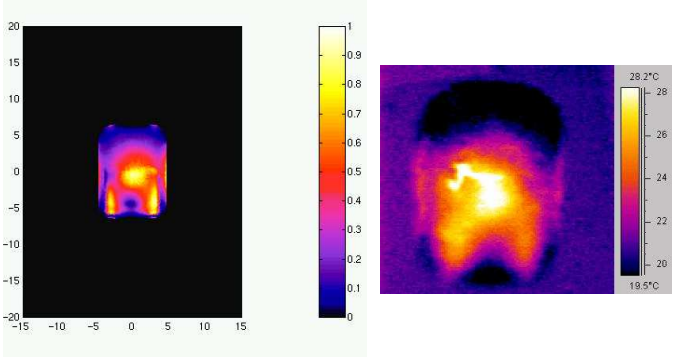

(a) Numerical (b) Thermal image

Fig. 18. Food surface plot at the base of the aluminium film package shown in figure 17.

A final configuration is considered where a thin film sheet comprising a complex arrangement of antenna structures, shown in figure 19, is used to create a more uniform heating distribution in a low loss food load (4.1 - j0.42).

The normalised absolute electric field and consequent power density distribution when no thin film surface is used, is shown in figure 20(a), for a convergence of 6.23%. A total of 278471 DOF was used and the simulation time was 9 hours and 9 minutes. The power density result highlights the non-uniform heating distribution within the asymmetrically positioned load geometry. When the patterned thin film surface is placed on the load surface, the DOF are increased to 279746. The hot spots are removed, as seen in figure 20(b), resulting in a more uniform heating pattern. The simulation required 9 hours and 37 minutes to reach a convergence of 10.215%.

VII. Conclusion

The paper has presented a new 3D edge element implementation of a discontinuous sheet for representing thin film surfaces.

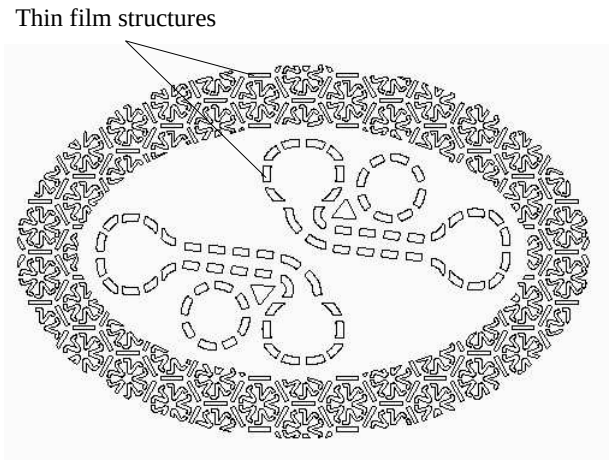

Fig. 19. Pattern of metallic antenna structures.

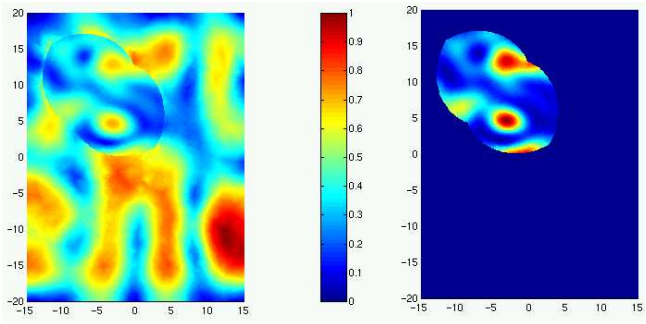

(a) Without thin film surface

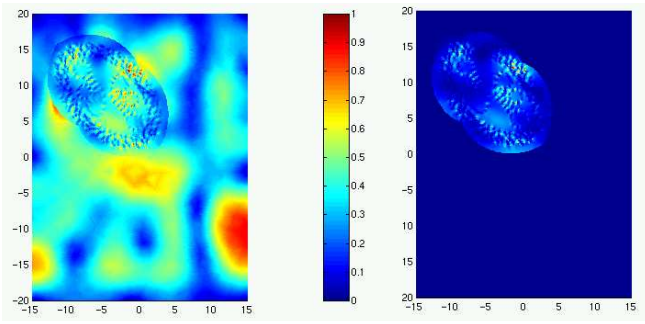

(b) With thin film surface

Fig. 20. Normalised absolute electric field (left) and power density pattern (right) on a plane through the multimode applicator (figure 14) that is coincident with the butter load surface.

This dual surface formulation has been described for both the frequency and time domain finite element methods. By comparison with three alternative boundary condition methods, the discontinuous sheet has been shown to yield results of superior accuracy. This is a consequence of including additional degrees of freedom in the set of unknown edge values which account for the field discontinuity across a thin film surface using standard transmission line theory.

A hybrid discontinuous-resistive sheet element has also been introduced for linking split elements of the thin film region with the surrounding mesh domain.

The use of the discontinuous sheet has been shown to be successful in characterising the performance of modern microwave heating applications incorporating active package technologies [9].

ACKNOWLEDGMENTS

The authors would like to acknowledge the assistance of Unilever Ltd., U.K., in providing active pack containers used for the validation of this work and to Dr. David Dibben of the Japanese Research Institute (JRI), Japan, for many helpful discussions.

REFERENCES

[1] M.A. Leontovich, "On the approximate boundary conditions for electromagnetic fields on the surface of well conducting bodies," *Investigations of Propagation of Radio Waves*, vol. B.A. Vvdensky, Ed. Moscow: Academy of Sciences USSR, pp. 5–20, 1948.

[2] J.M. Jin, J.L. Volakis, C.L. Yu, and A.C. Woo, "Modeling of resistive sheets in finite element solutions," *IEEE Transactions on Antennas and Propagation*, vol. 40, no. 6, pp. 727–731, June 1992.

[3] F. Bocquet, L. Pichon, A. Razek, and G. Tanneau, "3D FEM analysis of electromagnetic wave scattering from a dielectric sheet in EMC problems," *IEEE Transactions on Magnetics*, vol. 34, no. 5, pp. 2791–2794, 1998.

[4] S. Van den Berghe, F. Olyslager, and D. De Zutter, "Accurate modeling of thin conducting layers in FDTD," *IEEE Microwave and Guided Wave Letters*, vol. 8, no. 2, pp. 75–77, 1998.

[5] M. Feliziani and F. Maradei, "Edge element analysis of complex configurations in presence of shields," *IEEE Transactions on Magnetics*, vol. 33, no. 2, pp. 1548–1551, 1997.

[6] A.C. Metaxas, *Foundations of Electroheat A Unified Approach*, ISBN 0471956449, John Wiley & Sons, 1996.

[7] F. Alessandri and G. Baini and G. D'Inzeo and R. Sorrentino, "Conductor loss computation in multiconductor MIC's by transverse resonance technique and modified perturbational method," *IEEE Microwave and Guided Wave Letters*, vol. 2, no. 6, pp. 250–252, 1992.

[8] D. Dibben and A.C. Metaxas, "Frequency Domain vs. Time Domain Finite Element Methods for Calculation of Fields in Multimode Cavities," *IEEE Transactions on Magnetics*, vol. 33, no. 2, pp. 1468–1471, 1997.

[9] R.A. Ehlers, *Modelling of packaging systems in microwave fields*, Ph.D. thesis, University of Cambridge, 2001.

[10] W. Wood, *Practical time stepping schemes*, Clarendon Press, Oxford, U.K., 1990.

[11] D. Dibben and A.C. Metaxas, "Finite-Element Time-Domain Analysis of Multimode Applicators Using Edge Elements," *Journal of Microwave Power and Electromagnetic Energy*, vol. 29, no. 4, pp. 242–251, 1994.

[12] C. Habeger, "Microwave Interactive Thin Films," *Microwave World*, vol. 18, no. 1, pp. 8–22, 1997.

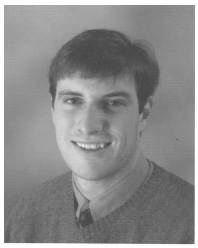

Richard Ehlers was born in Johannesburg, South Africa, in 1975. He received his B.Sc. Eng. (Elec.) and M.Sc. Eng. (Elec.) in 1996 and 1998 respectively, both from the University of the Witwatersrand, South Africa. His masters research focussed on the prediction of large air gap switching impulse breakdown voltages with an application to tower-conductor window configurations. Since 1997, he has been a member of the Electricity Utilisation Group at Cambridge University, U.K., involved with research into finite element modelling of thin films for microwave heating applications. He completed his Ph.D. in 2001 and continued the work on thin film modelling, which has also been licensed to industry, as a research associate at the Cambridge University Engineering Department. In addition to high voltage and electromagnetics, his research interests include avionics, aerial navigation and wireless communication systems. He is currently working in the area of system analysis and process definition of new and converted aircraft at Airbus Industry.

Ricky Metaxas is a Fellow and Tutor at St. John's College, Cambridge. He received his doctorate at Imperial College London in 1968. Besides his extensive teaching experience he has worked for the Atomic Energy Authority, the Electricity Council Research Centre (now EA Technology) and Eastern Electricity plc. He co-authored *Industrial Microwave Heating*, a book which is regarded as "the bible" for researchers working in the field of microwave heating. More recently he published a textbook, *Foundations of Electroheat : A Unified Approach*, which encompasses many aspects of electricity utilisation from ohmic heating to laser welding. He is a Fellow of the IEE and is currently President of AMPERE, a European based organisation devoted to the promotion of radio frequency and microwave energy and edits its Newsletter. He has co-authored over one hundred publications in many diverse areas such as electroheat, electricity utilisation, modelling of industrial heating systems and electromagnetics.